UC San Diego
UC San Diego Previously Published Works

Title

A microfluidic design for desalination and selective removal and addition of components in biosamples.

Permalink

https://escholarship.org/uc/item/9cz9918q

Journal

Biomicrofluidics, 13(2)

ISSN

1932-1058

Authors

Cai, Wei
Wang, Edward
Chen, Ping-Wei
et al.

Publication Date

2019-03-01

DOI

10.1063/1.5093348

Peer reviewed

A microfluidic design for desalination and selective removal and addition of components in biosamples

Wei Cai,[1,a] Edward Wang,[1,a] Ping-Wei Chen,[2] Yi-Huan Tsai,[1] Lennart Langouche,[3] and Yu-Hwa Lo[1,4,b]

AFFILIATIONS

[1]Materials Science and Engineering Program, University of California at San Diego, La Jolla, California 92093, USA
[2]Chemical Engineering Program, University of California at San Diego, La Jolla, California 92093, USA
[3]Department of NanoEngineering, University of California at San Diego, La Jolla, California 92093, USA
[4]Department of Electrical and Computer Engineering, University of California at San Diego, La Jolla, California 92093, USA

[a]**Contributions:** W. Cai and E. Wang contributed equally to this work.
[b]**Author to whom correspondence should be addressed:** ylo@ucsd.edu

ABSTRACT

We present the development of a microfluidic device that is able to selectively and nondisturbingly remove or add components to liquid samples, which allows control and conditioning of the samples for biomedical tests. The device consists of a series of chambers for sample retention and a through channel. Because smaller particles diffuse faster, small particles in the sample such as salt ions rapidly escape the chamber by diffusion and are subsequently removed by a carrier flow in the channel, leaving macromolecules of interest in the "desalted" solution. Conversely, components lacking in the sample can be diffused in by reversing the concentration gradient between the flow and the sample chamber. The ability to control the ionic strength of a sample offers many advantages in biological sample preparation as most biofluids contain high salt contents, making them unsuitable for downstream molecular analyses without additional sample treatments which could cause sample loss, contamination, and cost increase. Making use of the nature of laminar flow in a microfluidic device and mass transport by diffusion, we have developed an analytical model to calculate concentration profiles for different particles. Excellent agreements were found between the theory and the experiment, making the results highly reliable and predictable. Since the device and the principle is applicable to a wide range of biological samples, it can be incorporated into the workflow of various applications for research and *in vitro* diagnosis such as ion exchange, DNA sequencing, immuno assay, vesicle, cell secretion analysis, etc.

Published under license by AIP Publishing. https://doi.org/10.1063/1.5093348

INTRODUCTION

Sample preparation is required for nearly all biological and medical tests including DNA analysis [polymerase chain reaction (PCR), hybridization, and sequencing], protein analysis and immunoassays, vesicle and cell secretion analyses (exosomes, cytokines, and various macromolecules), microbes (bacteria and virus), and organelles (lysosomes, mitochondrial, chromatins, chromosomes, etc.). In most cases, the objects of interest contained in the biofluids cannot be directly applied to the tests without processing to condition the target objects in a proper environment.[1–5] One of the most common reasons for processing is control of the ionic strength of the sample. Most molecular tests require specific buffer and salt concentrations that are usually very different from the native biofluids.[6,7] For example, to make use of electrokinetic process such as dielectric electrophoretic process (DEP)[8–10] or electrophoresis (EP)[11] for enrichment, the high salt concentration of the biofluid can be a problem. For the simplest enrichment method by way of evaporation, an increase in salt concentration with reduced sample volume limits its utility although the method is simple and inexpensive.[12] For DNA hybridization in microarrays or solution based reactions, the desired hybridization buffers are very different from the native biofluids.

There have been quite a few designs that use diffusion properties to separate macromolecules or particles in fluid samples.

Examples include H-filter, T-sensor, lateral diffusion arrays, and microchambers.[13–15] However, these devices were designed for different purposes and unsuitable for biosample desalination and conditioning. An H-filter performs well when the two continuous streams move at an equal and steady velocity, a condition that is hard to maintain and unfeasible with a limited sample volume. Moreover, the H-filter may cause significant target dilution, adding difficulties in target enrichment post desalting.[16–18] T-sensors merge two fluid streams into a common channel to create a controlled diffusive interface.[13–15] T-sensors are ideal for measuring diffusivity and producing an environment for molecular reactions such as protein ligand binding, but they suffer from the same issues as H-filters when used for biosample desalting or conditioning. Other designs using diffusion effects include lateral diffusion arrays that use an applied electric field to create a well-defined molecules flow,[19] as well as devices with diffusion chambers[13–15] for cell culture[20–22] and lipid vesicles formation.[23,24] To summarize, although the idea of using diffusion or differential diffusivity to separate particles has been incorporated into many microfluidic devices, we have not found any design that is suitable for desalination and conditioning of biosamples for *in vitro* diagnosis such as protein, nucleic acid, and vesicle assays because those designs either take a large amount of sample which is often not available in real applications or have a limited ability for desalination due to the short amount of time the component in the medium stays in the device. Besides using diffusivity, there are also some microfluidic designs that use electrokinetics to achieve desalination.[25–28] However, those devices are complicated to fabricate and operate due to the electrodes and the required electric fields in fluid.

In this work, we present a simple microfluidic design that is able to selectively remove or separate components in a liquid sample by their diffusivity. The device consists of an array of parallel chambers connected to a fluidic channel. The sample in each chamber is in the "dead volume" of the laminar flow; therefore, the only mechanism of movement of the components in the sample is via diffusion against the concentration gradient. The concentration gradient is established by rapidly removing any component exiting the chamber by the carrier flow in the main channel. By keeping the sample in the "dead volume" next to the flow path, our device can maximize the concentration gradient which is suitable for samples of limited volume and allows ample time for out diffusion of ions to yield high desalination efficiency. Conversely, the carrier flow can also be used to bring extra components into the sample in the chamber via diffusion when the concentration gradient for the specific component is reversed. In addition to the high desalination efficiency, our design needs only one pump to introduce the flow from the inlet without special requirement for the flow speed, making the device much easier to operate than most existing devices. An analytical model has been developed to analyze the effectiveness of the process. Due to the exponential dependence of concentration on diffusivity, particles with a moderate diffusivity difference can produce several orders of magnitude difference in diffusion speed, thus making the process highly effective with minimum loss of the targets under proper control of the operation conditions. In order to experimentally validate the design, we used fluorescein salt, fluorescently labeled DNAs, and quantum dots/fluorescent beads to measure the concentration profile and the diffusivity of each component. The measured results were compared with the physical model that gives a closed form solution for the concentration profile with different device geometries and operation conditions.

MATERIALS AND METHODS

Device fabrication

The design was laid out using AutoCAD 2019. The main channel is $100\,\mu$m wide and $100\,\mu$m high. For the chambers, we have fabricated 3 different designs with depths of $250\,\mu$m, $350\,\mu$m, and $500\,\mu$m. All chambers have a width of $200\,\mu$m, a height of $100\,\mu$m, and a spacing of $100\,\mu$m with the neighboring chambers. The total length of the channel is 36 mm and the inlet/outlet holes are 1 mm in diameter. We used soft lithography process to fabricate the microfluidic device. To create the PDMS mold, 6-μm thick NR9-3000PY negative photoresist (Futurrex, Frankling, NJ, USA) was spin-coated on a 4-in. Si wafer at 800 rpm for 40 s. The wafer was soft baked at 150 °C for 1 min, followed by 90 s of UV exposure (Karl Suss MA6 Mask Aligner) and 100 °C post-exposure bake for 1 min. The patterns revealed after resist development. A 200-μm deep pattern was then etched by deep reactive ion etching (DRIE) process (Oxford Plasmalab 100) using the photoresist as the etch mask. In the DRIE process, SF_6 gas was flowed at 100 sccm for 11 s during the etching cycle, followed by a passivation cycle with C_4F_8 gas flowed at 80 sccm for 7 s. After the patterns were formed on the Si substrate, PDMS (Sylgard 184, Dow Corning, MI) was poured on the Si mold. The PDMS was then baked in a 65 °C oven for 2 h before demolding. To permanently bind the PDMS device to the glass substrate, oxygen plasma treatment was applied to the surface of both PDMS and glass. Then, the PDMS and glass slide were brought to contact and baked at 100 °C to enhance the binding strength. Harvard Apparatus Pico Plus Elite pumps were used to generate flow speeds of $10\,\mu$l/min for ion removal from and $1\,\mu$l/min for ion addition to the sample in the chambers.

Materials

The nanoparticles we used in this paper are 25 nm Q-dots (Qdot™ 545 ITK™ Streptavidin Conjugate Kit, Q10091MP) and 40 nm beads (FluoSpheres™ Carboxylate-Modified Microspheres, 0.04 μm, red fluorescent (580/605), 5% solids, azide free, F8793). The macromolecule we used is single-stranded FAM labeled DNA, 90 nt in length from Thermo Fisher. The salt we used is fluorescein sodium salt (Sigma-Aldrich, F6377).

Data processing and analysis

Images were taken by the Keyence BE-II 9000 fluorescent microscope and analyzed using ImageJ. We related the fluorescent intensity (I_t) to the concentration (C_t) by calibrating the response curves of the CMOS imager. The details are shown in the supplemental material. The parameter γ in Figs. 2 and 3 are defined as $\gamma = C_t/C_0$, where C_0 is the initial object concentration in the sample.

COMSOL fluidic mechanic simulation

Fluid flow profiles in microfluidic devices were modeled with COMSOL Multiphysics 5.2a using a stationary study with the laminar flow module to solve the incompressible Navier–Stokes equation. The three-dimensional geometry of the model was imported into COMSOL via a CAD file of the microfluidic device and the geometric model was divided into three sections: the inlet, body, and outlet. For the inlet parameters, the laminar inflow was at a flow rate of $10\,\mu$l/min with an entrance length of 1 m, while the outlet parameter was set to a pressure of 0. The walls of the device were set to no-slip boundary conditions. To ensure that the simulation was mesh-independent, mesh refinement was performed where the sizes of individual elements were successively reduced. Three successive simulations at increasingly finer element sizes (coarser, coarse, and normal) were completed and the resulting flow speeds were compared at a single area along the channel. For each simulation, there was no significant variation in flow speeds and the model corresponding to the coarser mesh (1 044 357 domain elements, 1 35 382 boundary elements, and 12 591 edge elements) was chosen for representation.

RESULTS AND DISCUSSION

Device design and characterization

The purpose of this device is for selective removal or addition of components while minimizing dilution of the sample and loss of target molecules through the exploitation of the considerable difference between the diffusivities of ions and macromolecules. A schematic of the device design and experiment flow is shown in Fig. 1. We start the experiment by filling the sample to all the chambers first, followed by flowing water at $10\,\mu$l/min through the channel. By controlling the duration of water flow, we can regulate the degree of desalting by diffusion. After desalting, we collect the sample from the chambers by vacuum. During vacuuming, we block the inlet and connect the outlet to a vacuum tube.

We have fabricated three different chamber depths: $\Delta = 250\,\mu$m, $\Delta = 350\,\mu$m, $\Delta = 500\,\mu$m, and all chambers are $200\,\mu$m wide and the flow channel is $100\,\mu$m wide. Both the chambers and the flow channel are $200\,\mu$m high. We choose the width and height by considering both desalting efficiency and practical factors including device fabrication process and chamber volume. We designed each chamber to have a volume of 10 and 20 nl. For devices consisting of 100 and 1000 chambers along the fluidic channel, the overall die size is around $6 \times 3\,\text{mm}^2$ and $1.2 \times 1.5\,\text{cm}^2$, respectively.

For sample desalting experiment, the chambers were first filled with 1.5 nM fluorescein sodium salt (Sigma-Aldrich, F6377) and then the channel was flowed with DI water at $10\,\mu$l/min, which yielded an average flow speed of 0.2 cm/s. In fact, the desalting results are not sensitive to the flow rate as long as it is much faster than the diffusion speed of the components. The above condition can be represented by the relation $D \ll vW$, where D is the component diffusivity in the sample, W and v are the width of the channel and the flow speed. At a flow speed of 0.2 cm/s and a chamber width of $200\,\mu$m, $vW \sim 4 \times 10^{-3}\,\text{cm}^2/s$, which is several orders of magnitude greater than the fastest diffusivity of any component in the sample. This means that at this flow speed, the concentration of any component at the junction of the chamber and the flow channel is almost zero, thus giving rise to the largest concentration gradient and the maximum desalting efficiency. The simulated flow velocity profile by COMSOL is shown in Fig. 1(c). As the fluorescein began to diffuse out of the chamber, the integrated fluorescent intensity of fluorescein sodium salt in each chamber decays exponentially over time. The parameter γ in Fig. 2 is defined as $\gamma = C_t/C_0$, where C_0 is the initial object concentration in the sample. The photobleaching effect of fluorescein was calibrated to be around 10% after 10 min experiment with 0.02 s exposure time, while the fluorescent intensity of the fluorescein salt in the chamber was reduced by nearly 10 000
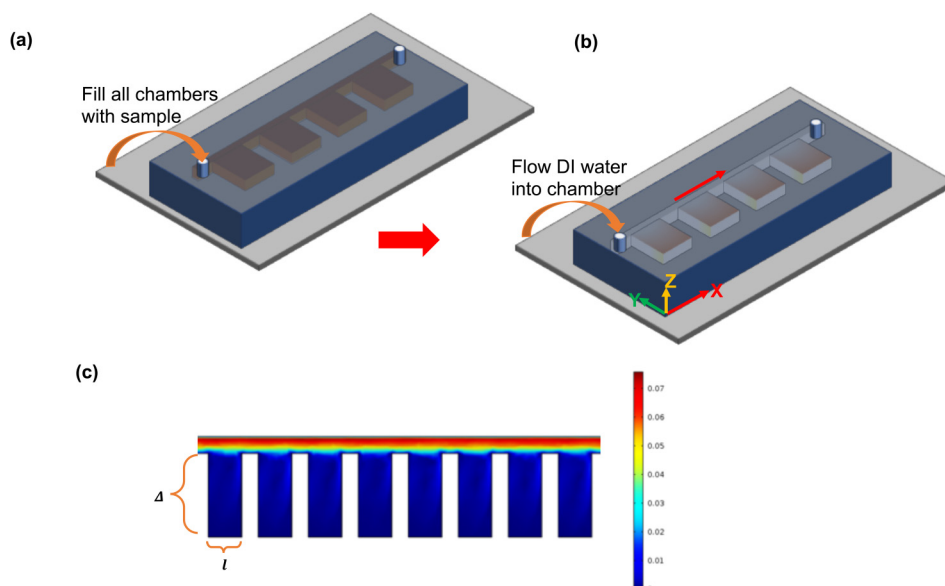

FIG. 1. Schematic illustration of device design and operation. (a) All chambers are first filled with the sample. (b) Flow DI water through the channel to establish a concentration gradient between the chamber and the channel for each component in the sample, which drives diffusion. If desired, components lacking in the original sample can be introduced to the chamber by establishing a reverse concentration gradient between the channel and the chamber (schematic not to scale). (c) Simulated fluid velocity distribution, indicating the samples in each chamber are in the dead volume (zero velocity). $l = 200\,\mu$m; $\Delta = 500\,\mu$m. Color scale bar: flow speed in m/s.
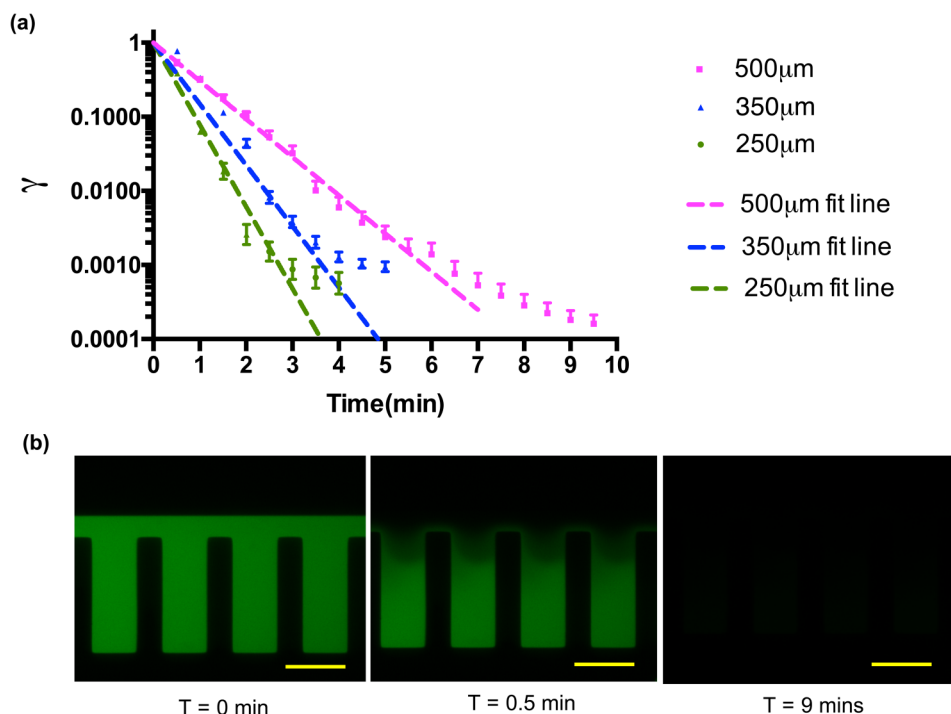
FIG. 2. (a) Time dependent fluorescein sodium salt concentration profile for different chamber depths: $\Delta = 250\,\mu m$, $350\,\mu m$, and $500\,\mu m$. The dashed line represents the fit line by an exponential function with a characteristic time constant. (b) Time lapse fluorescence image for $500\,\mu m$ deep chambers. The scale bar is $250\,\mu m$.

times. This demonstrates the effectiveness of desalting of our design. The detailed calibration of the photobleaching effect is included in the supplemental material. The experimental curve can be fitted by a characteristic time constant till the intensity reaches the camera noise floor, as shown in Fig. 2(a).

Experimentally, we observed that the flow velocity profile was extended into each chamber by as deep as $100\,\mu m$, which somewhat deviated from the simulation results for an ideal laminar flow. However, below this flow penetration depth, both experiment and simulation showed the true "dead volume," where the flow velocity
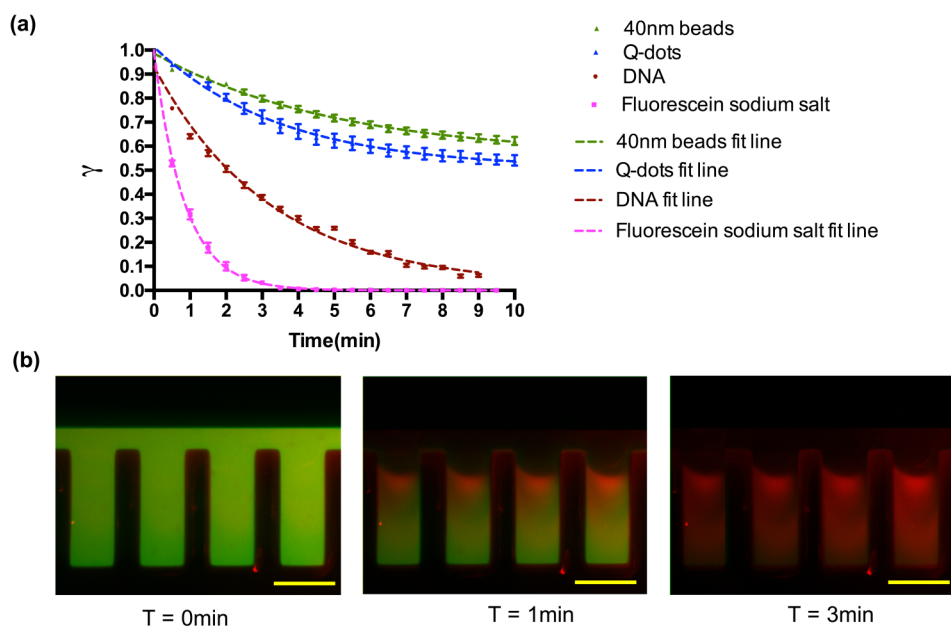

FIG. 3. (a) Time dependent concentration for 40 nm fluorescent bead, 25 nm Q-dots, fluorescent ssDNA (single-stranded FAM labeled DNA, 90 nt in length) and fluorescein sodium salt in $500\,\mu m$ chamber design. γ is the ratio of remaining particle concentration to original particle concentration in the chamber. (b) Time lapse fluorescent image for salt (green) and 40 nm beads (red). The scale bar is $250\,\mu m$. At 0 min, the fluorescence was dominated by that of fluorescent salt because of its much higher concentration. Over time, nearly all salt diffused out and only 40 nm beads remained in the chamber.
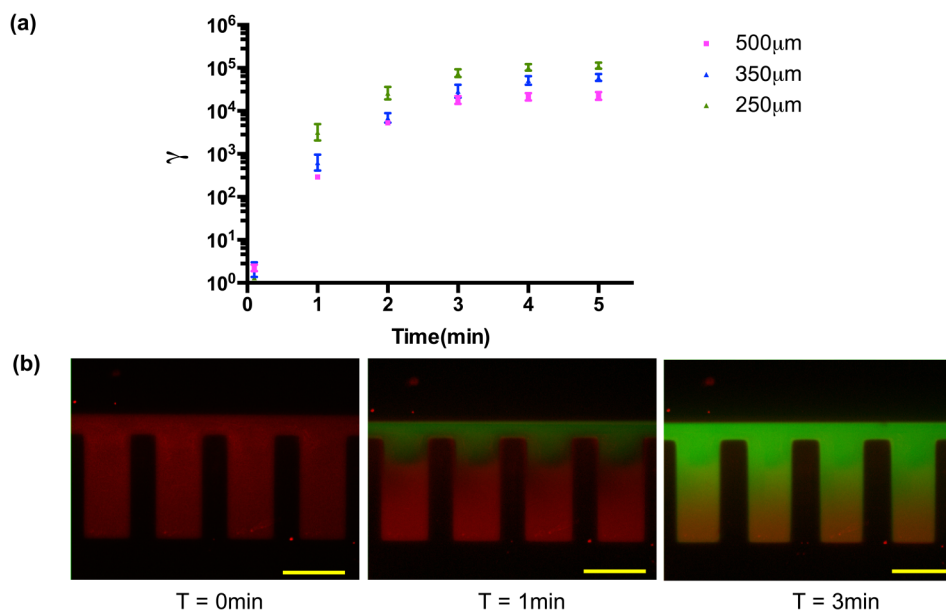
(a)

(b)

T = 0min   T = 1min   T = 3min

FIG. 4. Demonstration of introducing specific components into the sample in a controllable manner without increasing the sample volume. (a) Time dependent concentration of fluorescein sodium salt added to the chamber of different depths: $\Delta = 250\,\mu m$, $350\,\mu m$, $500\,\mu m$. γ is the ratio of fluorescein sodium salt relative to the initial amount in the sample. (b) Time lapse fluorescent images by adding salt into fluorescent ssDNA solution. Fluorescein sodium salt is in green color and fluorescent ssDNA is in red color. The scale bar is $250\,\mu m$.

was zero. Therefore, we confirmed that in positions deeper than $100\,\mu m$ in the chamber, the main working mechanism for particle movement was via diffusion.

To demonstrate the capability for selective removal of fast diffusive objects while keeping the slowly diffusive objects in the chamber, we measured the time dependent fluorescent intensity of different particles (fluorescein sodium salt, 40 nm beads, 25 nm quantum dots, and fluorescent single-stranded FAM labeled DNA, 90 nt in length) in a $500\,\mu m$ deep chamber. The time-dependent fluorescent intensities for the respective particles remaining in the chamber are shown in Fig. 3(a). Figure 3(b) shows the superimposed images for 40 nm beads (red) and fluorescein sodium salt (green). In 3 min, nearly all salt has diffused out of the chamber while greater than 80% nanobeads remain in the chamber. The process has produced a reliable and predictable concentration for specific objects in the sample, as predicted by the closed form solution of the diffusion equation described in the next section.

This device can also be used to add components to the sample without increasing the overall sample volume. To demonstrate this function, we reversed the process by flowing 1.5 nM fluorescein sodium salt into the chamber. Since the flow speed has minimum effects on the device performance, we use $1\,\mu l/min$ flow rate, to save the reagents. The chamber was prefilled with fluorescent ssDNA. As the fluorescein began to diffuse into the chamber, the integrated fluorescence intensity in the chamber increased. The results are shown in Fig. 4.

Physical model

In this section, we mathematically formulate the problem and obtain analytical solutions for the concentration profiles of particles with different diffusivities. The model provides a simple and accurate solution showing dependence of the solutions on all physical parameters explicitly.

The continuity equation for particles within a chamber in Fig. 1 can be written as

$$\frac{\partial n(x, y)}{\partial t} = -\frac{\partial}{\partial x}F_x - \frac{\partial}{\partial y}F_y, \tag{1}$$

where $n(x, y)$ is the particle concentration in each chamber ($0 \le x \le l$, $0 \le y \le \Delta$).

Assuming the sample in the chamber is in the dead volume of a laminar flow system, we have $v_x = 0$, $v_y = 0$ within the chamber. Therefore, only the diffusion terms contribute to the particle flux, and (1) can be simplified into (2) since the chamber geometry also produces the condition $\frac{\partial}{\partial x} = 0$,

$$\frac{\partial n(t, y)}{\partial t} = D\frac{\partial^2}{\partial y^2}n(t, y). \tag{2}$$

The following boundary conditions apply to the problem:

$$\frac{\partial n(t, y = 0)}{\partial y} = 0, \tag{3a}$$

$$n(t, \ y = \Delta) = 0. \tag{3b}$$

Here, $y = 0$ is at the end of the chamber and $y = \Delta$ is at the exit of the chamber, with Δ being the chamber depth. Equation (3b) is true when the DI water flow speed in the channel is much greater than the diffusion velocity such that particles exiting the chamber are immediately removed by the flow, leaving the particle concentration at the chamber exit to be nearly zero.

For the initial condition, we assume a uniform concentration profile within the chamber before the experiment starts,

$$n(t = 0, y) = n_o[u(y) - u(y - \Delta)], \tag{3c}$$

where $u(y)$ is the unit step function, n_o is the original particle concentration in the sample, and $t = 0$ (time when the water flow starts).

We assume a solution can be written in the form of $f(t)g(y)$. Substituting $f(t)g(y)$ into (2), we obtain

$$\frac{1}{f}\frac{df(t)}{\partial t} = \frac{\left[D\frac{d^2g}{dy^2}\right]}{g(x, y)} = -K.$$

The solutions of the above equation can be written as

$$f(t) = f(0)e^{-Kt},$$

$$g(y) = \cos\left(\sqrt{\frac{K}{D}}y\right).$$

Here, we drop the other possible solution $\sin\left(\sqrt{\frac{K}{D}}y\right)$ for $g(y)$ because it does not satisfy the boundary condition (3a).

For $g(y) = \cos\left(\sqrt{\frac{K}{D}}y\right)$ to satisfy the boundary condition (3b), we require

$$\sqrt{\frac{K}{D}}\Delta = \frac{\pi}{2}(2n + 1).$$

The allowed values for K are

$$K_n = D\left[\frac{\pi}{2\Delta}(2n + 1)\right]^2 \quad n = 0, \ 1, \ 2, \ \ldots. \tag{4}$$

Then, the solution $f(t)g(y)$ can be written as

$$f(t)g(y) = f(0)e^{-K_n t}\cos\left(\frac{\pi}{2\Delta}(2n + 1)y\right). \tag{5}$$

The general solution for (2) can be represented as

$$n(t, y) = \sum_0^\infty A_n e^{-K_n t} \cos\left[\frac{\pi}{2\Delta}(2n + 1)y\right]. \tag{6}$$

Using the initial condition (3c), we find

$$A_n = \frac{n_o \int_0^\Delta \cos\left[\frac{\pi}{2\Delta}(2n + 1)y\right]dy}{\int_0^\Delta \cos^2\left[\frac{\pi}{2\Delta}(2n + 1)y\right]dy} = n_o\frac{4}{(2n + 1)\pi}(-1)^n. \tag{7}$$

By substituting (7) into (6), we get the solution for (2) that satisfies the boundary and initial conditions

$$n(t, y) = n_o\sum_0^\infty \frac{4}{(2n + 1)\pi}(-1)^n e^{-\left[\frac{\pi}{2\Delta}(2n+1)\right]^2 Dt} \cos\left[\frac{\pi}{2\Delta}(2n + 1)y\right]. \tag{8}$$

Integrating (8) over the depth (Δ) of the chamber,

$$N(t) = \int_0^\Delta n(t, y)dy = n_o\Delta\sum_0^\infty \frac{8}{(2n + 1)^2\pi^2}e^{-\left[\frac{\pi}{2\Delta}(2n+1)\right]^2 Dt}. \tag{9}$$

The fraction of the component left in the sample after a time

TABLE I. Diffusion coefficient of different solutes.

Solute	D (cm²/s)
Fluorescein sodium salt	1.99×10^{-5}
ssDNA (90 nt)	5.19×10^{-6}
Q-dots (25 nm)	4.83×10^{-6}
40 nm beads	3.32×10^{-6}

duration "t" becomes

$$\gamma = \frac{N(t)}{n_o\Delta} = \sum_0^\infty \frac{8}{(2n + 1)^2\pi^2}e^{-\left[\frac{\pi}{2\Delta}(2n+1)\right]^2 Dt}. \tag{10}$$

For an approximate solution, we keep only the $n = 0$ term in (10) because after a long enough time period that satisfies the condition $\left[\frac{\pi}{2\Delta}\right]^2 Dt > 1$, all higher order ($n > 0$) terms decay to a much lower value than the $n = 0$ term. Thus,

$$\gamma = \frac{N(t)}{n_o\Delta} \sim \frac{8}{\pi^2}e^{-\left[\frac{\pi}{2\Delta}\right]^2 Dt} \quad \text{when} \quad \left[\frac{\pi}{2\Delta}\right]^2 Dt > 1. \tag{11}$$

Therefore, from the fraction of specific component left in the chamber after a certain time period, we can determine the diffusivity of the component. The diffusion coefficients, calculated from Eq. (11) and listed in Table I, fit the experimental data in Figs. 2(a) and 3(a) very well.

CONCLUSIONS

We have demonstrated the use of differential diffusivity of components in a fluid to condition liquid samples in a microfluidic device. The technique helps us achieve desired environments for testing of target particles from biofluids. The method is particularly suitable for removing/adding components to adjust the ionic strength and buffer condition for downstream analysis as ions usually have higher diffusivity than the nanoparticles such as exosomes and extracellular vesicles and macromolecules such as proteins and DNAs. Most uniquely, the method does not require target capture and release during the process of changing the buffer, thus avoiding uncontrollable sample loss, contamination, and human intervention. The physical model accurately matches the experimental results and helps control the process and produce predictable results. Therefore, the method provides an attractive option to be incorporated into the workflow of biological sample preparation for biomedical tests such as detection of nucleic acids from hybridization, immunobinding, and protein detection which require control and adjustment of ionic concentration and buffer condition. In addition, the method can be an effective means to measure the diffusivity of objects in the sample, which offers valuable insight for the physical properties of macromolecules such as their radius of hydration and geometry in different microenvironments.

SUPPLEMENTARY MATERIAL

See the supplementary material for more details of fluorescent intensity to concentration calibration and photobleaching effect of fluorescein.

REFERENCES

[1]W. Chen, J. M. Smeekens, and R. Wu, Nat. Commun. **9**, 1692 (2018).

[2]A. Isogawa, R. P. Fuchs, and S. Fujii, Sci. Rep. **8**, 5925 (2018).

[3]Q. Liu, C. Deng, and N. Sun, Nanoscale **10**, 12149–12155 (2018).

[4]Y. Li, C. Deng, and N. Sun, Anal. Chim. Acta **1024**, 84–92 (2018).

[5]M. Flaender, R. Den Dulk, V. Flegeau, J. Ventosa, G. Delapierre, J. Berthier, and A. Bourdat, Sens. Actuators B Chem. **258**, 148–155 (2018).

[6]M. Tokuyama, T. Moriki, and Y. Kimura, Phys. Rev. **83**, 051402 (2011).

[7]H. Chen, A. Stubbins, and P. G. Hatcher, Limnol. Oceanogr. Methods **9**, 582–592 (2011).

[8]H. Shafiee, J. L. Caldwell, and R. V. Davalos, J. Assoc. Lab. Autom. **15**, 224–232 (2010).

[9]P. Boc and K. Klepa, BioEssays **32**, 218–226 (2010).

[10]S. Li, M. Li, K. Bougot-Robin, W. Cao, I. Chau, W. Li, and W. Wen, Biomicrofluidics **7**, 024106 (2013).

[11]J. W. Zheng and X. Chong, Microsyst. Technol. **18**, 97–102 (2012).

[12]G. M. Walker and D. J. Beebe, Lab Chip **2**, 57–61 (2002).

[13]D. A. Beard, J. Appl. Phys. **89**, 4667–4669 (2001).

[14]A. Hatch, A. E. Kamholz, K. R. Hawkins, M. S. Munson, E. A. Schilling, B. H. Weigl, and P. Yager, Nat. Biotechnol. **19**, 461–465 (2001).

[15]A. Hatch, E. Garcia, and P. Yager, Proc. IEEE **92**, 126–139 (2004).

[16]E. Article, C. M. Dobson, T. P. J. Knowles, and G. Meisl, Chem. Sci. **9**, 3503–3507 (2018).

[17]Y. Zhang, A. K. Buell, T. Muller, E. De Genst, J. Benesch, C. M. Dobson, J. Knowles, and P. Tuomas, ChemBioChem **17**, 1920–1924 (2016).

[18]J. L. Osborn, B. Lutz, E. Fu, P. Kauffman, D. Y. Stevens, and P. Yager, Lab Chip **10**, 2659–2665 (2010).

[19]M. Cabodi, Y. Chen, S. W. P. Turner, H. G. Craighead, and R. H. Austin, Electrophoresis **23**, 3496–3503 (2002).

[20]A. You, M. A. Y. Be, and I. In, AIP Adv. **5**, 041310 (2015).

[21]K. Liu, R. Pitchimani, D. Dang, K. Bayer, T. Harrington, and D. Pappas, Langmuir **24**, 5955–5960 (2008).

[22]C. Luo, X. Zhu, T. Yu, and X. Luo, Biotechnol. Bioeng. **101**, 190–195 (2008).

[23]S. Vrhovec, M. Mally, B. Kavcic, and J. Derganc, Lab Chip **11**, 4200–4206 (2011).

[24]V. A. Online, M. Mally, S. V. Hartman, S. Mur, S. Svetina, and J. Derganc, RSC Adv. **7**, 36506–36515 (2017).

[25]B. Kim, R. Kwak, H. Kwon, V. Pham, M. Kim, B. Al-Anzi, G. Lim, and J. Han, Sci. Rep. **6**, 31850 (2016).

[26]S. J. Kim, S. H. Ko, R. Kwak, J. D. Posner, K. H. Kang, and J. Han, Nanoscale **4**, 7406–7410 (2012).

[27]M. Kim, M. Jia, and T. Kim, Analyst **138**, 1370–1378 (2013).

[28]B. Gumuscu, A. S. Haase, A. M. Benneker, M. A. Hempenius, A. Berg, R. G. H. Lammertink, and J. C. T. Eijkel, Adv. Funct. Mater. **26**, 8685–8693 (2016).